2018

The C terminus of the bacterial multidrug transporter EmrE couples drug binding to proton release

Nathan E. Thomas

Chao Wu

Emma A. Morrison

Anne E. Robinson

Jospehine P. Werner

See next page for additional authors

Authors

Nathan E. Thomas, Chao Wu, Emma A. Morrison, Anne E. Robinson, Jospehine P. Werner, and Katherine A. Henzler-Wildman

The C terminus of the bacterial multidrug transporter EmrE couples drug binding to proton release

Received for publication, August 17, 2018, and in revised form, September 25, 2018 Published, Papers in Press, October 4, 2018, DOI 10.1074/jbc.RA118.005430

Nathan E. Thomas[‡], **Chao Wu**[§], **Emma A. Morrison**[§1], **Anne E. Robinson**[§2], **Josephine P. Werner**[‡], and **Katherine A. Henzler-Wildman**[‡§3]

From the [‡]*Department of Biochemistry, University of Wisconsin-Madison, Madison, Wisconsin 53706 and* [§]*Department of Biochemistry and Molecular Biophysics, Washington University School of Medicine, St. Louis, Missouri 63110*

Edited by Karen G. Fleming

Ion-coupled transporters must regulate access of ions and substrates into and out of the binding site to actively transport substrates and minimize dissipative leak of ions. Within the single-site alternating access model, competitive substrate binding forms the foundation of ion-coupled antiport. Strict competition between substrates leads to stoichiometric antiport without slippage. However, recent NMR studies of the bacterial multidrug transporter EmrE have demonstrated that this multidrug transporter can simultaneously bind drug and proton, which will affect the transport stoichiometry and efficiency of coupled antiport. Here, we investigated the nature of substrate competition in EmrE using multiple methods to measure proton release upon the addition of saturating concentrations of drug as a function of pH. The resulting proton-release profile confirmed simultaneous binding of drug and proton, but suggested that a residue outside EmrE's Glu-14 binding site may release protons upon drug binding. Using NMR-monitored pH titrations, we trace this drug-induced deprotonation event to His-110, EmrE's C-terminal residue. Further NMR experiments disclosed that the C-terminal tail is strongly coupled to EmrE's drug-binding domain. Consideration of our results alongside those from previous studies of EmrE suggests that this conserved tail participates in secondary gating of EmrE-mediated proton/drug transport, occluding the binding pocket of fully protonated EmrE in the absence of drug to prevent dissipative proton transport.

Substrate binding and release are critical components of the mechanistic cycle for ion-coupled transporters. In single-site alternating access transport, a single binding site is alternately exposed to either side of the membrane, effectively transporting bound substrate across the membrane. Cooperative binding between substrate and ion increases the likelihood of cotransport (symport), whereas competition between substrate and ion favors antiport. Pure exchange of substrate and ion results when two conditions are met: 1) if binding of substrate excludes stable binding of the ion and vice versa and 2) if alternating access of the transporter is only permitted when substrate or ion is bound (see Fig. 1, *left*). This simple, attractive model elegantly explains stoichiometric antiport of ion and substrate and excludes alternative pathways that would result in dissipative leak of the driving ion (1, 2). However, the inherent difficulty in performing biochemistry and structural biology on membrane proteins has limited our ability to rigorously test the assumptions of the pure exchange model with a variety of transporters. Our recent studies of the small multidrug resistance transporter EmrE show that this drug/proton antiporter can simultaneous bind both substrates, violating the simplifying assumptions of the pure exchange model.

EmrE effluxes a wide range of aromatic cation antibiotics using the proton motive force across the inner membrane of *Escherichia coli*, thus conferring resistance to antibiotics matching this chemical profile (3). EmrE performs antiport of drug and proton through a classic single-site alternating access mechanism (4). The common binding site for drug and proton is defined by a pair of glutamates (Glu-14; one from each monomer within the homodimer; see Fig. 2) located deep within the membrane (5, 6). This binding site is alternately exposed to the cytoplasm and periplasm through conformational exchange of EmrE during the transport cycle (5, 7). EmrE's ease of purification, broad substrate specificity, and antiparallel topology have led to its adoption as a model system for studying multidrug efflux, membrane protein evolution, and secondary active transport (8–10). In addition to facilitating genetic analysis, EmrE's small size makes it an ideal candidate for NMR, allowing unprecedented structure-function investigations of an ion-coupled transporter. NMR has been used to confirm EmrE's antiparallel topology (11, 12), measure the rates of conformational exchange (alternating access) (13), probe the effects of drug or proton binding on EmrE's structure and dynamics (14, 15), and determine pK_a values for both Glu-14 residues (16, 17). Through these studies, it has become clear that EmrE's transport cycle is populated by more states than are included in pure exchange antiport.

This work was supported by National Institutes of Health Grant 1R01GM095839, National Institutes of Health National Research Service Award T32 GM007215 (to N. E. T.), National Science Foundation Graduate Research Fellowship DGE-1143954 (to E. A. M. and A. E. R.), and a Mr. and Mrs. Spencer T. Olin Fellowship for Women in Graduate Study (to A. E. R.). The authors declare that they have no conflicts of interest with the contents of this article. The content is solely the responsibility of the authors and does not necessarily represent the official views of the National Institutes of Health.

This article was selected as one of our Editors' Picks.

This article contains Figs. S1–S8 and Table S1.

[1] Present address: Dept. of Biochemistry, University of Iowa Carver College of Medicine, Iowa City, IA 52242.

[2] Present address: Division of Infectious Diseases, Dept. of Internal Medicine, Washington University School of Medicine, St. Louis, MO 63110.

[3] To whom correspondence should be addressed. E-mail: henzlerwildm@wisc.edu.

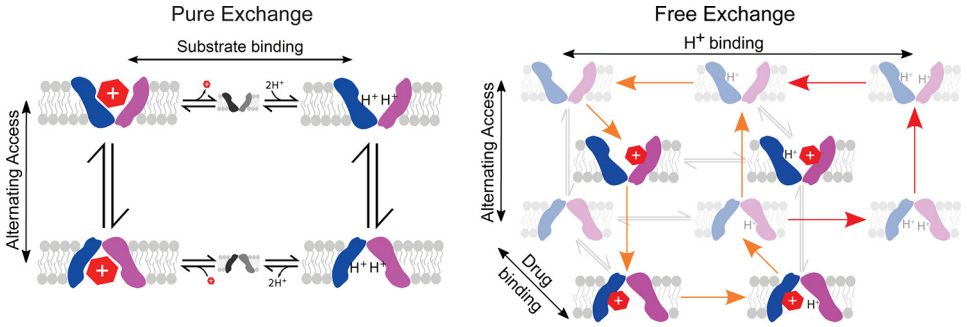

Figure 1. Two competing models for antiport. In pure exchange (*left*), strict competition for the single site between drug and two protons, along with prohibition of alternating access in the absence of substrate or ion, leads to tightly coupled stoichiometric antiport of $2H^+$/drug. In free exchange, competition remains, but no restrictions are placed on binding or alternating access, allowing both $1H^+$/drug (*orange*) and $2H^+$/drug (*red*) antiport.

Recently, we proposed a new "free exchange" kinetic model for coupled proton/drug transport by EmrE that includes all experimentally observed states and transitions of the transporter (Fig. 1, *right*) (17). In this model, there are multiple pathways around the transport cycle leading to different possible transport stoichiometries, including symport, antiport, and uniport of both drug and proton. Nevertheless, EmrE does not allow rapid proton leak in the absence of drug (17). Furthermore, binding of proton and drug to the single site is competitive: drug binding to one Glu-14 lowers the proton affinity (pK_a) of the second Glu-14, promoting proton release (17), whereas protonation of the second Glu-14 lowers the drug affinity (raises the K_D) of the first Glu-14, promoting drug release (17, 18). This competition is critical for ensuring that proton/drug antiport is the dominant transport process for common EmrE substrates under physiological conditions, leading to its well-established function as a proton-coupled drug efflux pump (19). Here, we further investigated this important competition between drug and protons by examining drug-induced proton release from EmrE. The results are generally consistent with the free exchange model but suggest that an additional residue may release protons upon drug binding. We trace this deprotonation event to His-110, EmrE's C-terminal residue and the only residue other than Glu-14 that has a pK_a value near neutral pH (16).

High-resolution structures of EmrE in different states of the transport cycle would shed light on the coupling mechanism between substrate binding and transport. However, the conformational plasticity that enables EmrE to transport diverse substrates also makes it a very challenging system for high-resolution structural studies (15, 20). As a result, there are currently only low-resolution cryo-EM (21, 22) and X-ray structures available (23) for the antiparallel EmrE homodimer (Fig. 2). The one region of EmrE that is not visible in these structures is the C-terminal tail. Terminal regions of proteins are frequently missing from crystal structures due to their dynamic nature and lack of regular structure. However, the NMR spectra of EmrE reveal that the C-terminal region of EmrE is not just a floppy tail. The residues in this region, including 105–110, have very unique chemical shifts that are not typical of α-helix or random coil, and the peaks are not as intense as they would be in an unstructured tail (11, 14). In addition, residues in this tail are sensitive to the occupancy of the binding pocket, with significant chemical shift perturbations upon protonation or drug binding (Fig. S1) (14). Finally, His-110 is highly conserved (Fig. S2) (24–26), indicating that it may be functionally important. Here, we show that the C-terminal tail of EmrE is strongly coupled to the binding domain, suggesting a potential role in secondary gating of EmrE transport.

Results

Modeling drug-induced proton release

Because drug and proton compete for binding to EmrE, addition of drug to EmrE triggers the release of protons from Glu-14 that can be directly measured with a pH electrode in a weakly buffered environment. In an earlier study, addition of a constant, low concentration of tetraphenylphosphonium (TPP^+)[4] to EmrE across a range of pH values produced a bell-shaped proton-release profile (27). This provided experimental confirmation of competitive binding between drug and proton for the first time in a solubilized transporter. However, these experimental conditions cannot distinguish between pure exchange and free exchange models. This is because drug and proton compete for binding to Glu-14 in both models, consistent with a weaker K_D^{app} for TPP^+ binding to EmrE at low pH when proton concentration is high (5, 17). Thus, addition of a low concentration of drug will not be sufficient to compete with and trigger release of protons from EmrE at low pH under either model.

If sufficient drug is added to saturate EmrE at all pH conditions, then the number of protons released upon drug binding to EmrE as a function of pH has a very different profile for the pure exchange and free exchange models (Fig. 3). Because the pure exchange model forbids simultaneous binding of drug and proton, any protons bound to the EmrE dimer initially will be released upon addition of a saturating concentration of drug. Thus, the number of protons released per EmrE dimer is simply the fraction of EmrE protonated in the drug-free state at the start of the experiment.

[4] The abbreviations used are: TPP^+, tetraphenylphosphonium; ITC, isothermal titration calorimetry; TM, transmembrane helix; TROSY, transverse relaxation optimized spectroscopy; HSQC, heteronuclear single-quantum coherence; HMBC, heteronuclear multiple bond correlation spectroscopy; SMR, small multidrug resistance; MD, molecular dynamics; DMPC, dimyristoylphosphatidylcholine; DLPC, dilauroylphosphatidylcholine; DHPC, dihexanoylphosphatidylcholine; Bicine, *N*,*N*-bis(2-hydroxyethyl)glycine; TCEP, tris(2-carboxyethyl)phosphine; BES, 2-[bis(2-hydroxyethyl)amino] ethanesulfonic acid.

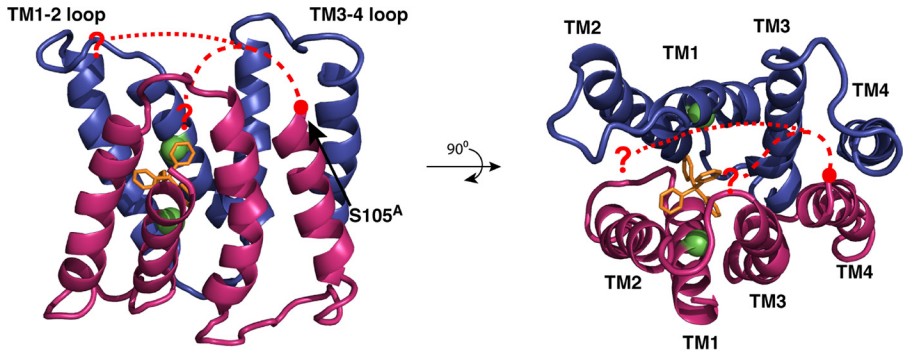

Figure 2. Structure of TPP^+-bound EmrE. The crystal structure (Protein Data Bank code 3B5D) (23) with monomer A in *magenta*, monomer B in *blue*, and TPP^+ in *orange* is shown. The C^α of Glu-14 is shown as a *green sphere*. The final residue in the structure, Ser-105^A, is indicated by a *red dot*. The location of the C-terminal tail is unknown, but it could interact with positively charged residues in the monomer B loops (*dotted line*) or fold into the binding pocket itself (*dashed line*).

$$\text{protons released} = \frac{2 \cdot 10^{pH^2} + 10^{pH \cdot pK_{a1}}}{10^{pH^2} + 10^{pH \cdot pK_a} + 10^{pK_a^2}} \quad \text{(Eq. 1)}$$

We assume cooperative proton binding reflected by a single pK_a of 7.3, in agreement with previous studies suggesting a pure exchange mechanism with a single pK_a for drug-free EmrE (13, 18, 28). Allowing asymmetric protonation of drug-free EmrE with two pK_a values for Glu-14, as shown by NMR (16), simply decreases the slope of the curve for proton release as a function of pH. In either case, at low pH where EmrE is fully protonated in the absence of drug, addition of a saturating drug concentration leads to the release of two protons (Fig. 3*A*, *black*).

For the free exchange model, the number of protons released upon drug binding can be calculated from the difference in Glu-14 protonation states in the presence and absence of drug.

$$\text{protons released} = (2EH_2 + EH^-) - EDH \quad \text{(Eq. 2)}$$

The net protonation state of EmrE in each condition is readily calculated using the Glu-14 pK_a values (Table 1 and Equations 3–5). These pK_a values were determined from NMR pH titrations of drug-free EmrE at 25 and 45 °C (16), TPP^+-bound EmrE at 45 °C (17), and TPP^+-bound EmrE at 25 °C (Figs. S3 and S4).

$$EH_2 = \frac{10^{pH^2}}{10^{pH^2} + 10^{pH \cdot pK_{a1}} + 10^{pK_{a1} \cdot pK_{a2}}} \quad \text{(Eq. 3)}$$

$$EH^- = \frac{10^{pH \cdot pK_{a1}}}{10^{pH^2} + 10^{pH \cdot pK_{a1}} + 10^{pK_{a1} \cdot pK_{a2}}} \quad \text{(Eq. 4)}$$

$$EDH = \frac{10^{-pH}}{10^{-pH} + 10^{-pK_{a3}}} \quad \text{(Eq. 5)}$$

At low pH, the free exchange model allows simultaneous binding of one drug and one proton, so only one proton will be released (Fig. 3*A*, *blue* and *red*) instead of the two protons predicted by the pure exchange model. To experimentally distinguish these two models, we first needed to establish the TPP^+ concentration necessary to saturate EmrE across the entire pH range.

Determination of pH-dependent TPP^+ binding affinity

We used isothermal titration calorimetry (ITC) to determine the K_D^{app} for TPP^+ binding to EmrE solubilized in isotropic bicelles at pH 5.5, 6.5, 7.5, or 8.5 and 45 °C. The titration profile observed at pH 5.5 with ITC directly confirms that saturation of the binding site with TPP^+ can be achieved even at low pH. Furthermore, the ITC data confirm that one drug binds per asymmetric dimer at all pH values (Table S1) as expected for TPP^+ binding to the single site defined by Glu-14 in EmrE (30). Using these experimentally determined K_D^{app} values, we calculated the concentration of TPP^+ needed to bind at least 99% of EmrE present in the proton-release assay at each pH value.

Measurement of proton release by ITC

In addition to the thermodynamics of drug binding, ITC can provide an indirect but robust measurement of proton release (31–33). The enthalpy observed upon drug binding (ΔH^0_{obs}) includes both the heat of reaction for protein–drug binding and consequent proton release as well as the enthalpy change due to released protons binding to the buffer. By measuring the standard enthalpy change (ΔH^0_{obs}) upon drug binding in multiple buffers with varying heats of ionization (ΔH^i_b), the number of protons released upon drug binding can be determined from the slope of ΔH^i_b *versus* ΔH^0_{obs} as described in detail previously (17).

We measured ΔH^0_{obs} of TPP^+ binding to EmrE solubilized in isotropic bicelles from pH 5.5–8.5 at 45 °C using at least three buffers at each pH (Table S1 and Fig. 3, *C* and *E*). If drug and proton binding were exclusive, as predicted by pure exchange, we would expect to see the release of two protons per dimer at low pH. Instead, slightly more than one proton is released per dimer at pH 5.5 in agreement with our previous experimental observation that EmrE can simultaneously bind drug and proton. However, the data are not perfectly consistent with the free exchange model: more protons are released than predicted near neutral pH (Fig. 3*A*, *red*). The free exchange model considers only Glu-14 protonation and deprotonation events as previous mutagenesis studies only implicated Glu-14 in drug and proton binding by EmrE (5, 6, 27), and Glu-14 is the only protonatable residue within the transmembrane helices that define the substrate-binding pore in EmrE (Fig. 2). Before considering the possibility that another residue may also participate in coupled binding/release of drug and protons, we first confirmed our experimental observation that the number of protons released upon TPP^+ binding is inconsistent with an Glu-14–only model

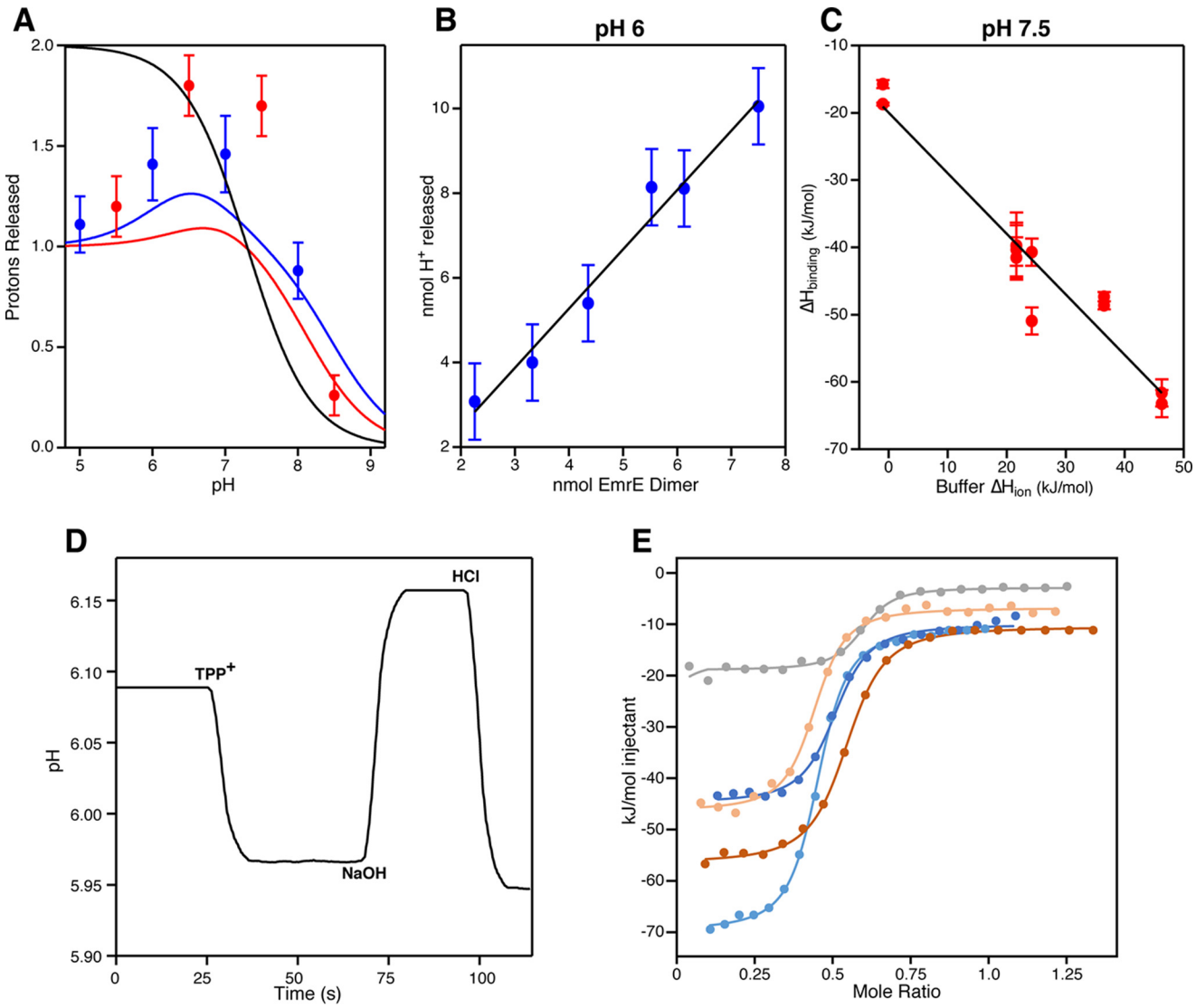

Figure 3. Glu-14 alone cannot account for drug-induced proton release. *A*, proton release per EmrE dimer upon addition of saturating concentration of TPP^+ as predicted by pure exchange (*black line*) or free exchange models of transport at 25 (*blue line*) or 45 °C (*red line*), assuming Glu-14 is the only residue involved. Experimental proton release, whether measured directly at 25 °C (*blue circles*) or by ITC at 45 °C (*red circles*), is more consistent with the free exchange model at low pH where the two models are most distinct. However, more protons are released upon TPP^+ binding near neutral pH than would be predicted by the Glu-14–only free exchange model. *Error bars* indicate the S.E. of the fit of proton release at each pH value. *B*, fit of proton release measured directly at 25 °C and pH 6 by pH electrode as a function of EmrE concentration. The slope indicates the drug-induced proton release per dimer (sample data shown in *D*), and the *error bars* indicate the S.D. of standard HCl aliquots. *C*, fit of enthalpy of TPP^+ binding as a function of buffer ionization enthalpy at 45 °C and pH 7.5. The negative slope represents the proton release per monomer (sample data shown in *E*). *Error bars* indicate the S.E. in the fit of $\Delta H_{binding}$. *D*, representative trace of TPP^+-induced proton release at pH 6. At the indicated time point, 5 μmol of TPP^+ was added to a solution containing 7.5 nmol of EmrE dimer, causing a release in protons seen by the drop in pH. This pH drop was converted to nmol of H^+ by the subsequent addition of known quantities of NaOH and HCl to the solution. Additional aliquots of HCl and NaOH were added to improve quantitation (data not shown). *E*, overlay of representative ITC binding curves for TPP^+ at 45 °C and pH 7.5 in either potassium phosphate (*gray*), BES (*dark blue*), MOPS (*beige*), imidazole (*brown*), or Tris (*light blue*) buffer (see Table S1 for complete ITC data).

using a different experimental approach and at a lower temperature (25 °C).

Direct measurement of drug-induced proton release

In the original investigation of drug-induced proton release (27), 4 μM aliquots of TPP^+ were added to weakly buffered EmrE solubilized in detergent, and pH changes were monitored and quantified directly using an electrode. We repeated this experiment using EmrE solubilized in bicelles and with 5 mM TPP^+ (Fig. 3, *B* and *D*), a concentration sufficient to saturate EmrE at all pH values based on our ITC experiments at 45 °C. We have previously shown that K_D^{app} decreases with temperature (11). Thus, this TPP^+ concentration will also be sufficient to saturate EmrE at 25 °C where the drug binds more tightly. Upon monitoring proton release in this manner, we again found that EmrE releases around one proton per dimer at low pH but releases more protons than expected near neutral pH (Fig. 3*A*, *blue*). When considered alongside the ITC experiments, this strongly suggests that a second residue, other than Glu-14, releases protons upon binding of drug to EmrE.

Which other residue could be involved in the coupled binding and release of drug and protons? The previous investigation of drug-induced proton release considered Glu-25 and Asp-84 (27) and found that they do not contribute to proton release.

Table 1
pK_a values for Glu-14 and His-110 determined by NMR

Residue	Drug-free	TPP^+-bound
25 °C		
Glu-14[a]	6.8 ± 0.1 (16)	6.32 ± 0.02[b]
Glu-14[a]	8.5 ± 0.2 (16)	
$His\text{-}110^A$	7.05 ± 0.02[c]	6.77 ± 0.03[c]
$His\text{-}110^B$	6.98 ± 0.01[c]	6.97 ± 0.03[c]
C-terminal tail A	N/A[d]	6.34 ± 0.04[b]
C-terminal tail B	N/A	7.00 ± 0.04[b]
45 °C		
Glu-14[a]	7.0 ± 0.1 (16)	6.8 ± 0.1 (17)
Glu-14[a]	8.2 ± 0.3 (16)	

[a] Drug-free EmrE pK_a values are macroscopic pK_a values and cannot be unambiguously assigned to $Glu\text{-}14^A$ or $Glu\text{-}14^B$. The pK_a value for TPP^+-bound EmrE is due to protonation of $Glu\text{-}14^B$.
[b] Determined by TROSY-HSQC monitoring backbone amide chemical shift change with pH (Figs. S3 and S4). For the C-terminal tail, chemical shift perturbations of Ser-105, Arg-106, and Thr-108 fit to the reported pK_a values (Fig. S4).
[c] His-110 pK_a value of the side chain imidazole determined from a pH titration with HMBC NMR spectra (Fig. 5 and Figs. S6 and S7).
[d] N/A, not applicable.

This is consistent with our more recent NMR-monitored pH titration experiments, which do not show any titration of Asp-25 or Glu-84 near physiological pH. Instead, the only residue other than Glu-14 that titrates near neutral pH in our NMR experiments is His-110 (16), which has not been previously considered in the proton-release mechanism. This C-terminal residue is highly conserved among EmrE-like members of the SMR family (Fig. S2) but has no known role in EmrE function. Could His-110 account for the elevated proton release?

Determination of His-110 pK_a

To test this hypothesis, we performed pH titrations of drug-free and TPP^+-bound EmrE using $^1H\text{-}^{15}N$ HMBC NMR experiments to directly observe the histidine side chain (Fig. S5) (34). Although HMBC experiments are relatively insensitive, the direct observation of the imidazole ring enables an accurate determination of the histidine side chain pK_a value. Conveniently, EmrE only has a single histidine residue, allowing clean observation of His-110 in this experiment.

At 45 °C, the rapid rate of alternating access in drug-free EmrE results in intermediate or fast exchange of the $His\text{-}110^A$ and $His\text{-}110^B$ peaks such that they are not resolved in the HMBC spectra, preventing accurate determination of the His-110 side chain pK_a values at that temperature. Fortunately, at 25 °C, the peaks corresponding to His-110 from each monomer in the asymmetric homodimer are clearly resolved (Fig. 4 and Figs. S5, S6, and S7), allowing the determination of the pK_a for $His\text{-}110^A$ and $His\text{-}110^B$ separately (Table 1 and Fig. 5). This reveals a drug-induced pK_a shift of $His\text{-}110^A$ (Table 1), which is in the C-terminal tail of EmrE located on the open side of the transporter. Interestingly, there is no drug-induced pK_a shift for $His\text{-}110^B$, which is located on the closed face. The pK_a shift of $His\text{-}110^A$ upon TPP^+ binding will result in the release of protons from this C-terminal residue. Including proton release from His-110 along with the proton release from Glu-14 in the free exchange model gives a better fit of the experimental proton-release data at 25 °C (Fig. 6).

Evidence for coupling of the C-terminal tail to the binding pocket

The drug-induced pK_a shift of $His\text{-}110^A$ (Table 1) and sensitivity of the C-terminal tail chemical shifts to the identity of the bound substrate (Fig. S1) could occur through direct interaction with the binding pocket or indirectly due to large-scale conformational change upon drug binding. To investigate this further, we reanalyzed the effect of pH on the backbone amide groups throughout EmrE as recorded in the $^1H\text{-}^{15}N$ TROSY-HSQC pH titration of TPP^+-bound EmrE (Fig. S3). We have previously shown that pH-dependent chemical shift perturbations of core residues in the binding pocket of drug-bound EmrE are the result of protonation of Glu-14 (16). As expected, residues in the tail of monomer B have pH-dependent chemical shift perturbations that are well-fit with a pK_a value matching the $His\text{-}110^B$ side chain pK_a value (Table 1 and Fig. S4). However, the pH-dependent chemical shifts of residues in the monomer A C-terminal tail have pK_a values that match the pK_a of Glu-14, not $His\text{-}110^A$. This strong coupling between the C-terminal tail of monomer A and Glu-14 suggests a more direct interaction of this tail with the core binding domain of EmrE, either with the binding pocket itself or with the structured loops surrounding the pocket (Fig. 2).

Assessing solvent accessibility of His-110

If the C-terminal tail of monomer A is interacting with the binding pocket in some way, it may be protected from water because the binding cavity is hydrophobic and poorly hydrated relative to the bulk aqueous solution (35). To analyze the solvent accessibility of the C terminus, we recorded spectra with and without a water-soluble paramagnetic ion, Mn^{2+} (Fig. 7). The Mn^{2+} will cause paramagnetic relaxation enhancement of nearby nuclei, leading to the disappearance of peaks in the NMR spectra that correspond to residues accessible to water. At high pH, the backbone amides of both $His\text{-}110^A$ and $His\text{-}110^B$ are in an aqueous environment because these peaks disappear in the presence of Mn^{2+}. However, at pH 5.2, the His-110 signals remain visible in the spectrum even in the presence of Mn^{2+}, indicating that His-110 is more protected from water at low pH (Fig. 7).

Evidence for a second state of $His\text{-}110^A$

At elevated pH, the $His\text{-}110^A$ peaks are broadened in the nitrogen dimension, indicative of microsecond to millisecond transitions between different conformational states. This is apparent to a certain extent for drug-free EmrE and is even more pronounced with TPP^+ bound. Although no second state is visible in the HMBC spectra, this pulse sequence is relatively insensitive and may not detect lowly populated states. To address this, we prepared TPP^+-bound EmrE selectively labeled with [^{13}C,^{15}N]histidine and acquired TROSY-HSQC spectra at pH 6 and 8 to observe the backbone amides. Because His-110 is the only histidine in EmrE, only peaks corresponding to His-110 are visible. The increased sensitivity of this pulse sequence reveals two peaks in addition to the major states of His-110, confirming that His-110 has multiple conformations when TPP^+ is bound (Fig. 8). It likely that His-110 also exists in multiple conformations for drug-free EmrE, but the highly

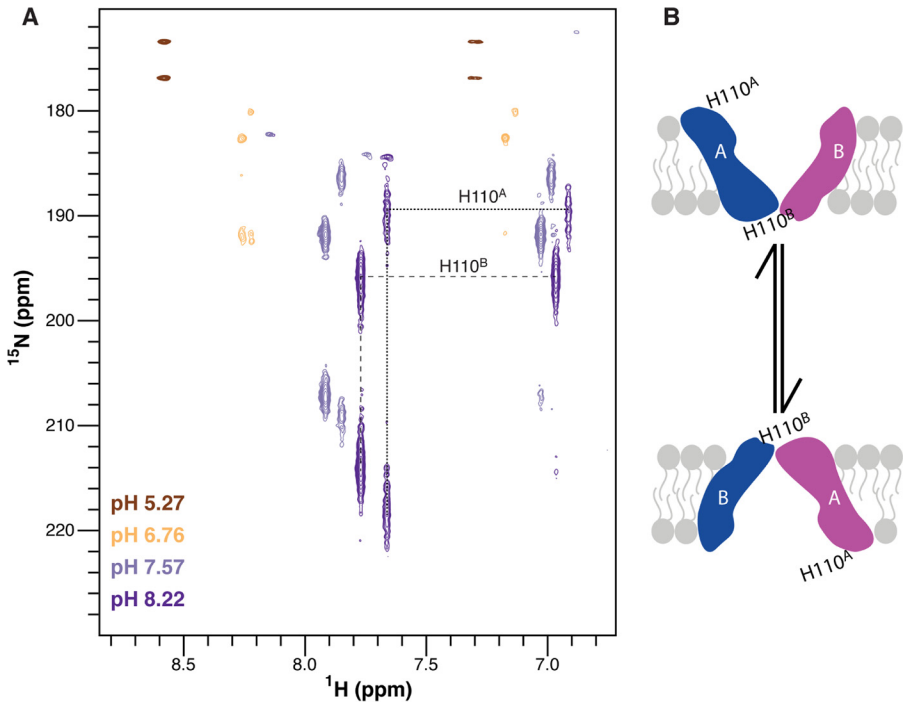

Figure 4. NMR-monitored pH titration of His-110 side chain. *A*, His-110 peaks for each monomer in HMBC NMR spectra of drug-free EmrE in isotropic bicelles are clearly resolved at 25 °C. Three or four peaks are observed for each imidazole ring as explained in Fig. S5. As pH changes, the peak positions titrate along a line, consistent with a single protonation event. The peak positions at low pH fall along this line for both monomers, indicating that the peak overlap at low pH is due to similar chemical environments for the two residues, not fast exchange. Thus, the pK_a for each monomer can be determined separately. Representative peaks are shown (see Fig. S6 for full titration). *B*, during alternating access conformational exchange, EmrE's antiparallel protomers swap conformation. Monomer A is defined as the protomer in which the N and C termini (His-110^{A}) are facing the same side of the membrane as the binding pocket regardless of whether EmrE is open-up or open-down.

dynamic nature of EmrE under these conditions makes this difficult to demonstrate conclusively.

Discussion

Ion-coupled transport requires regulated access of ions and substrates into and out of the binding site. Transport will be biased toward symport or antiport depending on whether ion and substrate binding is competitive or cooperative and how the relative rates of alternating access vary when the transporter is empty or bound to substrate and/or ion. Cartoon models of transporters often exclude states and transitions that would weaken coupling efficiency or lead to leak pathways, but few transporters have been studied in sufficient detail to unambiguously support their exclusion. Recently, it was shown that the H^+/sugar symporter GlcP is capable of H^+/sugar antiport in violation of traditional models of symport (36). Instead, the authors proposed a "universal" kinetic model of transport that can accommodate symport, antiport, or uniport depending on the rates of the transitions between the various states. This is similar to our free exchange model for EmrE. In the case of EmrE, the rates of alternating access in different substrate-bound and substrate-free states have previously been studied (13–17, 35) and do not follow the expected patterns for coupled antiport. Both NMR experiments and MD simulations indicate that apoEmrE is capable of alternating access (13, 16, 35), and NMR demonstrates that EmrE can simultaneously bind and transport drug and proton near neutral pH (17). Those results suggest that EmrE should be capable of both symport and antiport of drug and protons and should rapidly leak protons. Nevertheless, functional assays demonstrate that EmrE does not leak protons in the absence of drug. Furthermore, although liposomal transport assays indicate that EmrE may be capable of both symport and antiport, its well-established drug-resistance activity indicates that antiport is the dominant function under physiological conditions (17). Here, we focus on the competition between drug and proton binding to EmrE to see whether this matches the expectations for an ion-coupled antiporter.

The experiments presented here investigated the competitive binding of drug and protons to EmrE to better understand how this promiscuous transporter is biased toward net antiport. We have identified an additional protonatable residue coupled to drug binding, His-110, and demonstrate that the C-terminal tail of EmrE on the open side of the transporter is strongly coupled to the Glu-14 binding pocket within TM1–3. At first, a role for His-110 in EmrE's binding mechanism seems surprising. The C-terminal tail of EmrE extends from TM4, which mediates EmrE dimerization and is set apart from EmrE's core binding domain (TM1–3) (Fig. 2) (25). Previous Cys-scanning mutagenesis studies of EmrE did not reveal a significant role for the C-terminal tail in substrate binding or transport (6, 37, 38). However, His-110 is highly conserved across the SMR family (Fig. S2), suggesting an important but as yet undiscovered functional role. Consideration of our results alongside previous studies of EmrE suggests that this conserved tail may participate in secondary gating of EmrE transport, occluding the binding pocket of fully protonated EmrE in the absence of drug and preventing proton leak.

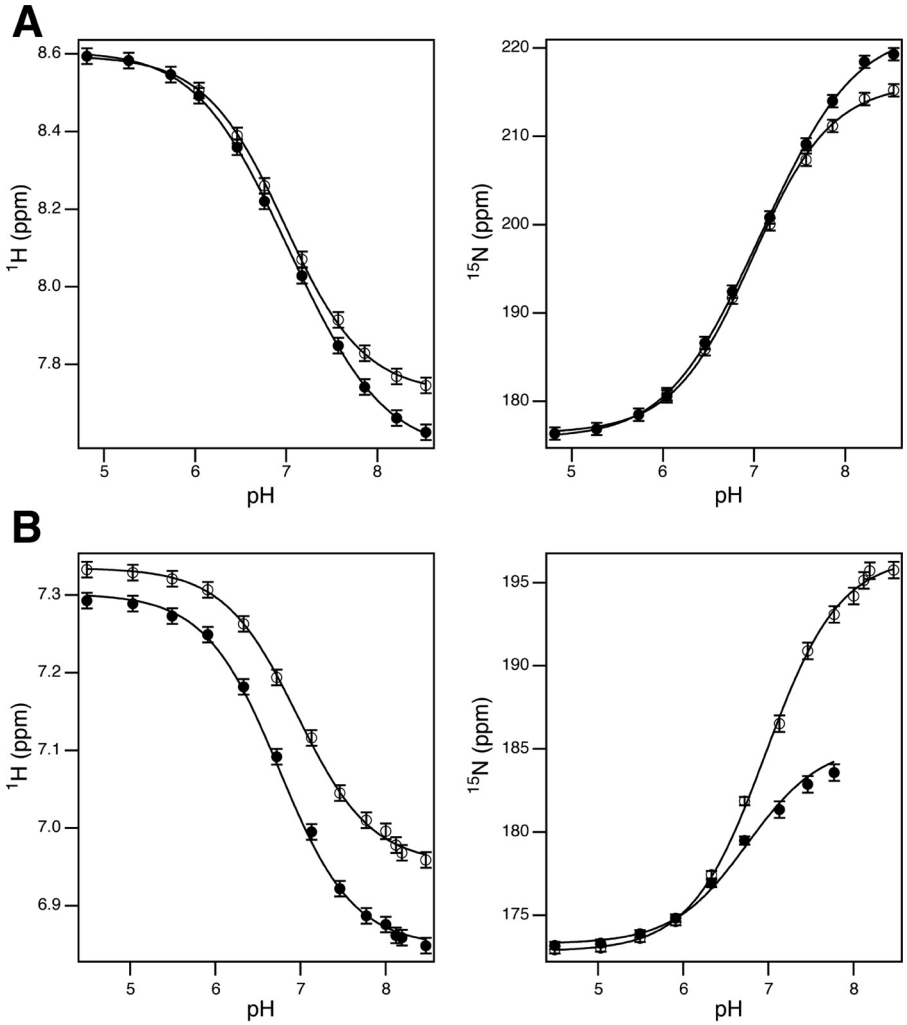

Figure 5. Determination of the His-110 side chain pK_a. *A*, the $H^{\delta 2}$ and $N^{\epsilon 2}$ chemical shifts of His-110^A (*filled*) and His-110^B (*open*) from the HMBC pH titration of drug-free EmrE are fit to determine the pK_a. $H^{\delta 2}$ and $N^{\epsilon 2}$ data were simultaneously fit to a single pK_a for each monomer individually. *B*, fit of His-110^A (*filled*) and His-110^B (*open*) from the HMBC pH titration of TPP^+-bound EmrE. Proton and nitrogen were fit together, but due to line broadening at high pH, there are no nitrogen data above pH 7.77 for His-110^A. A summary of pK_a values can be found in Table 1. *Error bars* indicate the peak width at half the maximum intensity.

To better understand the functional implications of competition between drug and proton binding to EmrE, we measured drug-induced proton release from EmrE as a function of pH (Fig. 3). At low pH, we observed the release of approximately one proton per dimer, which is consistent with the simultaneous binding of drug and proton by EmrE and the free exchange model. Surprisingly, around neutral pH, we observed greater proton release than could be explained by consideration of drug and proton binding at the established "single" binding site defined by Glu-14. Our prior NMR-monitored pH titrations showed that His-110 is the only other residue that titrates near neutral pH (16). We observed a drug-induced pK_a shift for the imidazole side chain of His-110^A in the presence and absence of TPP^+. Incorporating the proton release from His-110 into the model accounts for the increased proton release near neutral pH.

In addition to the drug-induced pK_a shift of His-110, the C terminus of EmrE is acutely sensitive to drug binding. These effects could be due to direct interaction of the C-terminal tail with the binding site near Glu-14 or indirectly through changes in the overall conformation when EmrE is bound to different drugs. The tail is not resolved in the available crystal and cryo-EM structures of EmrE (21, 23), preventing a direct structural analysis. Re-examination of our previous NMR pH titrations monitoring the backbone amides (Fig. S3) revealed that the backbone amides in tail A fit to a pK_a of 6.3, matching the pK_a of Glu-14 in the active site of TPP^+-bound EmrE (Table 1). The large pH-dependent chemical shifts displayed by these residues indicate a significant change in chemical environment, which could be consistent with a direct interaction with the binding domain. The poor solvent accessibility of His-110 at low pH for TPP^+-bound EmrE further indicates that the tail is located in a less exposed environment as would be the case if it folds back toward the active site (Fig. 2, *dashed line*). Interestingly, in a recent molecular dynamics study using a complete model of EmrE embedded in a lipid bilayer, the tail of monomer A existed in heterogeneous populations, some of which did extend back into the binding pocket for an extended period during the simulation (35). Our experimental results, including our observation of multiple states for His-110, are consistent with this MD simulation.

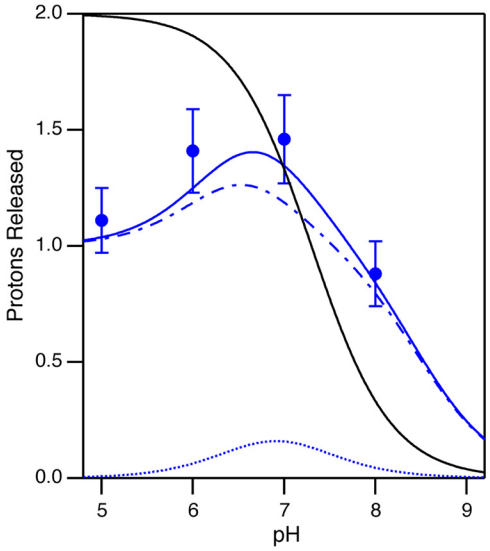

Figure 6. His-110 contributes to drug-induced proton release at 25 °C. Predicted proton release due to the drug-induced pK_a shift of Glu-14 (*dashed line*) or His-110 (*dotted line*) measured by NMR is shown. Including both Glu-14 and His-110 in the proton-release model (*solid line*) leads to increased proton release near neutral pH and gives a better fit of the data compared with an Glu-14 – only model (*dashed line*). *Error bars* indicate the S.E. of the fit of proton release at each pH value.

If the C-terminal tail can extend into the binding pocket, what is its role in the transport mechanism of EmrE? A possible functional mechanism for the C-terminal tail as a secondary gate in EmrE begins to emerge from consideration of our data and previously published experiments examining the structure and function of EmrE using a variety of experimental approaches.

In recent MD simulations, the binding pocket spontaneously dehydrated when both Glu-14 residues were protonated (35). This is in agreement with double electron– electron resonance EPR measurements, which showed repacking of the TM3-4 loop to occlude the binding pocket upon lowering the pH from 8 to 5 for drug-free EmrE (28). Interestingly, this pH-dependent conformational change was also observed in E14Q-EmrE, demonstrating that it must depend on the protonation of a residue other than Glu-14. The authors proposed protonation of Glu-25 and Asp-84 given the locations of these residues within the structure and the effect of mutations at these positions. Although this is a logical conclusion, there is no evidence for protonation of either Glu-25 or Asp-84 in this pH range in our NMR spectra, which provide a more direct probe of electrostatic environments (16). However, as shown here, His-110 does titrate in this pH range and is sensitive to drug binding. Additionally, both coevolutionary analysis and MD simulations suggest interactions between the C-terminal tail and the TM3-4 loop (Fig. S8). Furthermore, in the MD simulations, interactions were observed between His-110^A and the TM1-2 loop where Glu-25 is located. These interactions only occurred when EmrE was fully protonated or in an unstable singly protonated state that is likely physiologically irrelevant.

In consideration of these results, we propose that protonation of His-110^A at low pH could facilitate electrostatic interactions between positive charges in the C-terminal tail (His-110 and Arg-106) and the negatively charged Glu-25 and Asp-84 in the TM1-2 and TM3-4 loops (Fig. 2, *dotted line*). Formation of such an interaction upon His-110^A protonation could explain the pH-dependent conformational change of the TM3-4 loop to occlude the Glu-14 binding pocket observed by EPR at low pH and is consistent with the NMR pH titration data and evolutionary couplings. If the binding pocket is occluded when EmrE is fully protonated, it would prevent proton transport across the membrane in the absence of drug. This could explain the most significant shortcoming of the Glu-14-only free exchange model, the prediction that EmrE should rapidly transport protons across the membrane in the absence of drug in contrast to results from proton leakage assays that show no significant proton leak (17).

However, for EmrE to perform coupled antiport of drug and proton, proton transport must occur in the presence of drug. In an early NMR study of EmrE, TPP^+ binding to EmrE was monitored by ^{31}P NMR, allowing direct observation of the drug (40). In that study, two distinct populations of EmrE-bound TPP^+ were observed. At low concentrations, TPP^+ bound weakly to Glu-25 and Asp-84 via electrostatic interactions. Binding of TPP^+ to the canonical binding site at Glu-14 only occurred when the TPP^+:EmrE dimer ratio exceeded 1:1 even though this site has a higher affinity. We propose that the binding of TPP^+ to Glu-25 and Asp-84 observed at low drug concentrations (40) disrupts the electrostatic interactions between these residues and the positively charged C-terminal tail. This results in release of the C-terminal tail from interaction with the loops surrounding the transport, opening the secondary gate and allowing proton release from and drug binding to Glu-14 within the transport pore. Although speculative, this mechanism is consistent with the experimentally observed behavior of the loop and the tail of EmrE and would explain the tight kinetic correlation of drug on-rates and proton off-rates previously observed by stopped flow (18). Our proposed model is also analogous to a recently uncovered mechanism in MdfA, a multidrug/proton antiporter from the major facilitator superfamily with a remarkably similar substrate profile to EmrE in which electrostatic interactions between loop residues around the rim of the binding pocket are essential to proper gating of transport (41).

Although gating is a common feature of transporters (2, 42), the presence of a secondary gate in EmrE would be remarkable in a such a small transporter. At first glance, distinctions between secondary gating within a free exchange transport model and the pure exchange model of antiport might seem trivial because both mechanisms are gated, limiting proton transport in the absence of drug. However, gating EmrE at the fully protonated state, as proposed here, rather than the deprotonated state is a crucial distinction. In the pure exchange model, proton leak is prevented by stipulating that the empty transporter cannot alternate access. If EmrE *can* alternate access when deprotonated, as demonstrated by NMR (15, 16) and allowed in the free exchange model, then EmrE should confer drug sensitivity under certain conditions. Indeed, EmrE-mediated sensitivity to methyl viologen, a +2 substrate, has been demonstrated both at high pH (19) and at neutral pH when the Glu-14 pK_a is lowered by mutation to aspartate (13). This is consistent with electrogenic drug uptake. Additionally,

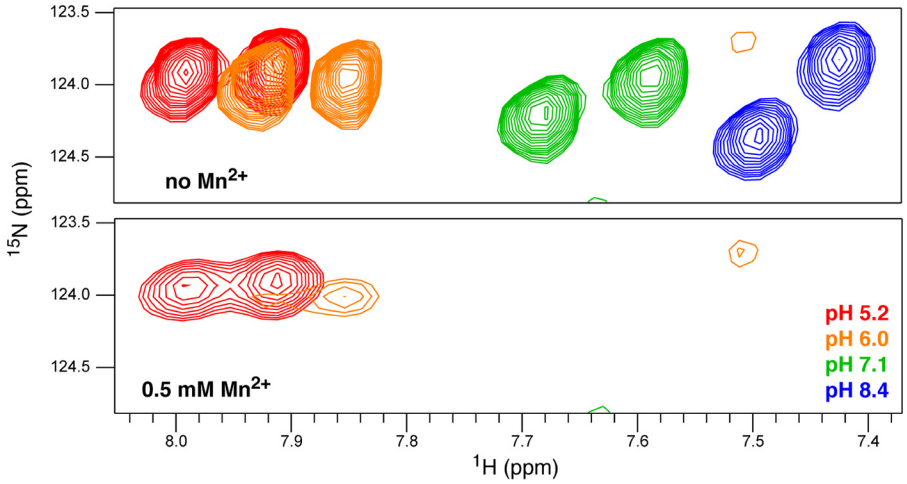

Figure 7. His-110 is protected from solvent at low pH. TROSY-HSQC NMR spectra of TPP^+-bound EmrE in the absence (*top*) and presence (*bottom*) of the paramagnetic ion Mn^{2+} (0.5 mM) are shown. At low pH, the His-110 signal is not fully relaxed by Mn^{2+}, indicating that it is at least partially protected from water under these conditions.

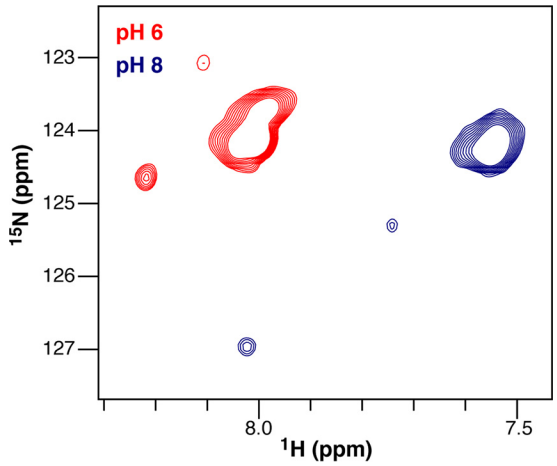

Figure 8. His-110 exists in multiple states when TPP^+ is bound. TROSY-HSQC spectra of TPP^+-bound EmrE selectively labeled with [^{13}C,^{15}N]histidine reveal at least two additional histidine peaks at both low and high pH. These could correspond to two additional states of His-110^A or one additional state each of both His-110^A and His-110^B.

this mechanism would explain the ease with which EmrE can be transformed from a proton-coupled efflux pump to a polyamine importer by a single point mutation, W63G (43). Such a mutation would not need to fundamentally alter the dynamics or mechanism of the transporter; it would merely need to change EmrE's binding specificity. Finally, this mechanism would represent an inversion of the strict competition stipulated by the pure exchange model. Rather than excluding simultaneous drug and proton binding, binding of drug, albeit to a secondary site, would be required for proton release. Competition between drug and proton remains central to antiport, but the mechanism may be very different from mechanisms proposed by earlier models.

Experimental procedures

Expression and purification

EmrE was expressed and purified as described previously (44). ^{15}N-Labeled samples were grown in M9 medium supplemented with 1g/liter $^{15}NH_4Cl$ (for HMBC experiments) or D_2O M9 medium supplemented with 0.5g/liter ^{15}N ISOGRO (Sigma-ISOTEC) and 1g/liter $^{15}NH_4Cl$ (for HSQC experiments). Histidine-labeled samples were grown in M9 medium with 33 mg/liter ^{13}C,^{15}N-labeled histidine added 1 h prior to induction. EmrE purified in *n*-decyl-β-D-maltopyranoside was reconstituted into DMPC or DLPC liposomes at a 1:80 EmrE monomer: lipid molar ratio. Detergent was removed by Amberlite XAD-2 beads, and liposomes were collected by ultracentrifugation. Samples were resuspended in NMR buffer containing DHPC at a 1:3 long chain to short chain lipid ratio to prepare isotropic bicelles.

Isothermal titration calorimetry

ITC titrations were performed in a TA Instruments Low Volume Nano calorimeter using the ITCRun software (TA Instruments, Lindon, UT) with 2.5-μl injections, stirring at 350 rpm at 45 °C. Each buffer condition was run two to four times with a minimum of three buffers per pH value between 5.5 and 8.5. At lower pH values, samples contained 20 mM buffer and 20 mM NaCl. At pH 8.5, all samples contained 50 mM buffer to improve buffering capacity and minimize pH drift. Buffer ionization enthalpies were adjusted to 45 °C using the reported standard molar heat capacity change at 25 °C (29). Each titration was analyzed independently, confirming the 1 TPP^+:EmrE dimer (n = 0.5 TPP^+/EmrE monomer) binding stoichiometry under all conditions. ITC experiments in MOPS at pH 7.5 were performed with both 20 and 50 mM MOPS to confirm that observed binding enthalpies were independent of buffer concentration. EmrE in 1:3 DLPC:DHPC isotropic bicelles ranged in concentration from 25 to 835 μM EmrE (monomer concentration), and TPP^+ concentrations varied from 76 μM to 5 mM TPP^+, depending on pH, to keep the *c*-value for the ITC experiment in an optimal range. Sample pH was checked at 45 °C before and after each experiment. Data are reported in Table S1. The data were fit as described previously (17, 39).

Modeling proton release

Proton release from Glu-14 was modeled as described in the main text. Proton release from His-110^A was similarly calculated by subtracting the fraction of protonated His-110^A in

TPP^+-saturated EmrE from the fraction of protonated His-110^A in drug-free EmrE where

$$\text{fraction of protonated H110}^A = \frac{10^{-pH}}{10^{-pH} + 10^{-pK_a}} \quad \text{(Eq. 6)}$$

using the relevant pK_a value from Table 1. The pK_a values for His-110^B were not significantly different, so no protons are released from His-110^B.

Direct measurement of proton release

EmrE in 1:3 DMPC:DHPC isotropic bicelles with 1 mM Bicine, 0.5 mM MOPS, 0.5 mM MES, 0.2 mM acetate, 100 mM NaCl was diluted with bicelles (80 mM DMPC, 240 mM DHPC) in the same buffer to create stock solutions ranging from 40 to 200 μM (monomer concentration) EmrE. 100-μl EmrE stock solutions were diluted with 800 μl of 7.5 mM DHPC, 100 mM NaCl, and precise concentrations were determined from the A_{280} (EmrE $\epsilon = 38{,}368\ M^{-1}\ cm^{-1}$) of this solution immediately before each experiment. 10 mM NaOH or HCl was used to bring each sample to the desired initial pH. 100 μl of 50 mM TPP^+ in 50 mM DHPC, 100 mM NaCl adjusted to the desired pH was added to saturate EmrE and initiate proton release. Proton release was monitored directly with a microelectrode using an HI 2209 analog pH meter from Hanna Instruments digitized with a DataQ data logger. Proton release was quantified by at least five subsequent additions of 20 nM HCl and NaOH per sample, and proton concentration was assumed to be linear within this range. A minimum of five concentrations of EmrE was used to monitor proton release at each pH, and a plot of measured proton release *versus* dimer concentration was used to generate reported values of proton release per dimer.

NMR pH titration

All pH titration data were collected using a Bruker Avance III HD 900-MHz spectrometer with a cryogenic probe on 0.6–1.0 mM EmrE samples in $q = 0.33$ DMPC:DHPC isotropic bicelles. Sample buffers contained 100 mM Bicine, 50 mM MOPS, 50 mM MES, 20 mM acetate, 20 mM NaCl, 2 mM TCEP, 6% D_2O, 0.05% NaN_3 with 4 mM TPP^+ added to drug-bound samples. Sample pH was adjusted using a pH electrode and was measured again after each NMR experiment to account for any pH drift. pH drifts during 2D NMR experiments were only observed for titration points above pH 8, and the average pH value was used. TROSY-HSQC spectra were collected as described previously (17). HMBC spectra were collected using a modified HSQC sequence with delays during insensitive nuclei enhanced by polarization transfer (INEPT) steps adjusted to suppress one-bond *J*-coupling and select for long-range coupling. Proton and nitrogen chemical shifts were fit using IgorPro (Wavemetrics) to the following equation to determine pK_a values.

$$\delta = \frac{\delta_H 10^{-pH} + \delta_D 10^{-pK_A}}{10^{-pH} + 10^{-pK_A}} \quad \text{(Eq. 7)}$$

where δ_H is the chemical shift of the protonated species at low pH, δ_D is the chemical shift of the deprotonated species at high pH, and pK_A is the pK_a of the titratable group. For drug-bound HMBC spectra of His-110, broadening of the monomer A peak in the nitrogen dimension prevented accurate peak position determination above pH 7.8. Proton peak positions above this pH were determined from 1D slices of the 2D HMBC spectra.

Paramagnetic relaxation analysis

Four separate uniformly labeled NMR samples were prepared as described in 100 mM MOPS, 100 mM Bicine, 20 mM acetate, 20 mM NaCl at different pH values. Samples contained 0.7 mM EmrE in $q = 0.33$ isotropic bicelles as well as 0.05% NaN_3, 10% D_2O, 2 mM TCEP, 2 mM TPP^+, 2 mM disuccinimidyl suberate. Each sample was adjusted for pH at 35 °C, and the pH was checked again after data acquisition. To assess paramagnetic relaxation effects, 0.5 mM $MnCl_2$ was added to each sample, and another, identical ^1H-^{15}N TROSY-HSQC spectrum was collected in the same manner.

Author contributions—N. E. T., C. W., E. A. M., and K. H.-W. conceptualization; N. E. T., E. A. M., A. E. R., and K. H.-W. data curation; N. E. T., C. W., E. A. M., and A. E. R. formal analysis; N. E. T., C. W., E. A. M., A. E. R., J. P. W., and K. H.-W. investigation; N. E. T., A. E. R., and J. P. W. visualization; N. E. T., C. W., E. A. M., and A. E. R. methodology; N. E. T. writing-original draft; N. E. T., E. A. M., and K. H.-W. writing-review and editing; K. H.-W. supervision; K. H.-W. funding acquisition; K. H.-W. project administration.

Acknowledgments—We thank Geoff Chang for the EmrE expression plasmid. This study made use of the National Magnetic Resonance Facility at Madison, which is supported by National Institutes of Health Grant P41GM103399 (NIGMS), old number: P41RR002301. Equipment was purchased with funds from the University of Wisconsin-Madison, the National Institutes of Health (P41GM103399, S10RR02781, S10RR08438, S10RR023438, S10RR025062, S10RR029220), the NSF (DMB-8415048, OIA-9977486, BIR-9214394), and the United States Department of Agriculture (USDA).

References

1. Forrest, L. R., Krämer, R., and Ziegler, C. (2011) The structural basis of secondary active transport mechanisms. *Biochim. Biophys. Acta* **1807,** 167–188 CrossRef Medline
2. Boudker, O., and Verdon, G. (2010) Structural perspectives on secondary active transporters. *Trends Pharmacol. Sci.* **31,** 418–426 CrossRef Medline
3. Yerushalmi, H., Lebendiker, M., and Schuldiner, S. (1995) EmrE, an *Escherichia coli* 12-kDa multidrug transporter, exchanges toxic cations and H^+ and is soluble in organic solvents. *J. Biol. Chem.* **270,** 6856–6863 CrossRef Medline
4. Schuldiner, S. (2009) EmrE, a model for studying evolution and mechanism of ion-coupled transporters. *Biochim. Biophys. Acta* **1794,** 748–762 CrossRef Medline
5. Muth, T. R., and Schuldiner, S. (2000) A membrane-embedded glutamate is required for ligand binding to the multidrug transporter EmrE. *EMBO J.* **19,** 234–240 CrossRef Medline
6. Yerushalmi, H., and Schuldiner, S. (2000) A common binding site for substrates and protons in EmrE, an ion-coupled multidrug transporter. *FEBS Lett.* **476,** 93–97 CrossRef Medline
7. Yerushalmi, H., and Schuldiner, S. (2000) An essential glutamyl residue in EmrE, a multidrug antiporter from *Escherichia coli*. *J. Biol. Chem.* **275,** 5264–5269 CrossRef Medline
8. Cymer, F., von Heijne, G., and White, S. H. (2015) Mechanisms of integral membrane protein insertion and folding. *J. Mol. Biol.* **427,** 999–1022 CrossRef Medline

9. Lloris-Garcerá, P., Seppälä, S., Slusky, J. S., Rapp, M., and von Heijne, G. (2014) Why have small multidrug resistance proteins not evolved into fused, internally duplicated structures? *J. Mol. Biol.* **426,** 2246–2254 CrossRef Medline
10. Schuldiner, S., Granot, D., Mordoch, S. S., Ninio, S., Rotem, D., Soskin, M., Tate, C. G., and Yerushalmi, H. (2001) Small is mighty: EmrE, a multidrug transporter as an experimental paradigm. *News Physiol. Sci.* **16,** 130–134 Medline
11. Morrison, E. A., DeKoster, G. T., Dutta, S., Vafabakhsh, R., Clarkson, M. W., Bahl, A., Kern, D., Ha, T., and Henzler-Wildman, K. A. (2011) Antiparallel EmrE exports drugs by exchanging between asymmetric structures. *Nature.* **481,** 45–50 CrossRef Medline
12. Gayen, A., Banigan, J. R., and Traaseth, N. J. (2013) Ligand-induced conformational changes of the multidrug resistance transporter EmrE probed by oriented solid-state NMR spectroscopy. *Angew. Chem. Int. Ed. Engl.* **52,** 10321–10324 CrossRef Medline
13. Gayen, A., Leninger, M., and Traaseth, N. J. (2016) Protonation of a glutamate residue modulates the dynamics of the drug transporter EmrE. *Nat. Chem. Biol.* **12,** 141–145 CrossRef Medline
14. Morrison, E. A., and Henzler-Wildman, K. A. (2014) Transported substrate determines exchange rate in the multidrug resistance transporter EmrE. *J. Biol. Chem.* **289,** 6825–6836 CrossRef Medline
15. Cho, M.-K., Gayen, A., Banigan, J. R., Leninger, M., and Traaseth, N. J. (2014) Intrinsic conformational plasticity of native EmrE provides a pathway for multidrug resistance. *J. Am. Chem. Soc.* **136,** 8072–8080 CrossRef Medline
16. Morrison, E. A., Robinson, A. E., Liu, Y., and Henzler-Wildman, K. A. (2015) Asymmetric protonation of EmrE. *J. Gen. Physiol.* **146,** 445–461 CrossRef Medline
17. Robinson, A. E., Thomas, N. E., Morrison, E. A., Balthazor, B. M., and Henzler-Wildman, K. A. (2017) New free-exchange model of EmrE transport. *Proc. Natl. Acad. Sci. U.S.A.* **114,** E10083–E10091 CrossRef Medline
18. Adam, Y., Tayer, N., Rotem, D., Schreiber, G., and Schuldiner, S. (2007) The fast release of sticky protons: kinetics of substrate binding and proton release in a multidrug transporter. *Proc. Natl. Acad. Sci. U.S.A.* **104,** 17989–17994 CrossRef Medline
19. Rotem, D., and Schuldiner, S. (2004) EmrE, a multidrug transporter from *Escherichia coli*, transports monovalent and divalent substrates with the same stoichiometry. *J. Biol. Chem.* **279,** 48787–48793 CrossRef Medline
20. Korkhov, V. M., and Tate, C. G. (2008) Electron crystallography reveals plasticity within the drug binding site of the small multidrug transporter EmrE. *J. Mol. Biol.* **377,** 1094–1103 CrossRef Medline
21. Ubarretxena-Belandia, I., Baldwin, J. M., Schuldiner, S., and Tate, C. G. (2003) Three-dimensional structure of the bacterial multidrug transporter EmrE shows it is an asymmetric homodimer. *EMBO J.* **22,** 6175–6181 CrossRef Medline
22. Fleishman, S. J., Harrington, S. E., Enosh, A., Halperin, D., Tate, C. G., and Ben-Tal, N. (2006) Quasi-symmetry in the cryo-EM structure of EmrE provides the key to modeling its transmembrane domain. *J. Mol. Biol.* **364,** 54–67 CrossRef Medline
23. Chen, Y.-J., Pornillos, O., Lieu, S., Ma, C., Chen, A. P., and Chang, G. (2007) X-ray structure of EmrE supports dual topology model. *Proc. Natl. Acad. Sci. U.S.A.* **104,** 18999–19004 CrossRef Medline
24. Brill, S., Sade-Falk, O., Elbaz-Alon, Y., and Schuldiner, S. (2015) Specificity determinants in small multidrug transporters. *J. Mol. Biol.* **427,** 468–477 CrossRef Medline
25. Elbaz, Y., Salomon, T., and Schuldiner, S. (2008) Identification of a glycine motif required for packing in EmrE, a multidrug transporter from *Escherichia coli*. *J. Biol. Chem.* **283,** 12276–12283 CrossRef Medline
26. Ninio, S., Rotem, D., and Schuldiner, S. (2001) Functional analysis of novel multidrug transporters from human pathogens. *J. Biol. Chem.* **276,** 48250–48256 CrossRef Medline
27. Soskine, M., Adam, Y., and Schuldiner, S. (2004) Direct evidence for substrate-induced proton release in detergent-solubilized EmrE, a multidrug transporter. *J. Biol. Chem.* **279,** 9951–9955 CrossRef Medline
28. Dastvan, R., Fischer, A. W., Mishra, S., Meiler, J., and Mchaourab, H. S. (2016) Protonation-dependent conformational dynamics of the multidrug transporter EmrE. *Proc. Natl. Acad. Sci. U.S.A.* **113,** 1220–1225 CrossRef Medline
29. Goldberg, R. N., Kishore, N., and Lennen, R. M. (2002) Thermodynamic quantities for the ionization reactions of buffers. *J. Phys. Chem. Ref. Data* **31,** 231–370 CrossRef
30. Tate, C. G., Ubarretxena-Belandia, I., and Baldwin, J. M. (2003) Conformational changes in the multidrug transporter EmrE associated with substrate binding. *J. Mol. Biol.* **332,** 229–242 CrossRef Medline
31. Kozlov, A. G., and Lohman, T. M. (2000) Large contributions of coupled protonation equilibria to the observed enthalpy and heat capacity changes for ssDNA binding to *Escherichia coli* SSB protein. *Proteins* **41,** Suppl. 4, 8–22 Medline
32. Armstrong, K. M., and Baker, B. M. (2007) A comprehensive calorimetric investigation of an entropically driven T cell receptor-peptide/major histocompatibility complex interaction. *Biophys. J.* **93,** 597–609 CrossRef Medline
33. Baker, B. M., and Murphy, K. P. (1996) Evaluation of linked protonation effects in protein binding reactions using isothermal titration calorimetry. *Biophys. J.* **71,** 2049–2055 CrossRef Medline
34. Pelton, J. G., Torchia, D. A., Meadow, N. D., and Roseman, S. (1993) Tautomeric states of the active-site histidines of phosphorylated and unphosphorylated I11 Glc, a signal-transducing protein from Escherichia coli, using two-dimensional heteronuclear NMR techniques. *Protein Sci.* **2,** 543–558 Medline
35. Vermaas, J. V., Rempe, S. B., and Tajkhorshid, E. (2018) Electrostatic lock in the transport cycle of the multidrug resistance transporter EmrE. *Proc. Natl. Acad. Sci. U.S.A.* **115,** E7502–E7511 CrossRef Medline
36. Bazzone, A., Zabadne, A. J., Salisowski, A., Madej, M. G., and Fendler, K. (2017) A loose relationship: incomplete H^+/sugar coupling in the MFS sugar transporter GlcP. *Biophys. J.* **113,** 2736–2749 CrossRef Medline
37. Mordoch, S. S., Granot, D., Lebendiker, M., and Schuldiner, S. (1999) Scanning cysteine accessibility of EmrE, an H^+-coupled multidrug transporter from *Escherichia coli*, reveals a hydrophobic pathway for solutes. *J. Biol. Chem.* **274,** 19480–19486 CrossRef Medline
38. Amadi, S. T., Koteiche, H. A., Mishra, S., and McHaourab, H. S. (2010) Structure, dynamics, and substrate-induced conformational changes of the multidrug transporter EmrE in liposomes. *J. Biol. Chem.* **285,** 26710–26718 CrossRef Medline
39. Sigurskjold, B. W. (2000) Exact analysis of competition ligand binding by displacement isothermal titration calorimetry. *Anal. Biochem.* **277,** 260–266 CrossRef Medline
40. Glaubitz, C., Gröger, A., Gottschalk, K., Spooner, P., Watts, A., Schuldiner, S., and Kessler, H. (2000) ^{31}P-CP-MAS NMR studies on TPP^+ bound to the ion-coupled multidrug transport protein EmrE. *FEBS Lett.* **480,** 127–131 CrossRef Medline
41. Zomot, E., Yardeni, E. H., Vargiu, A. V., Tam, H.-K., Malloci, G., Ramaswamy, V. K., Perach, M., Ruggerone, P., Pos, K. M., and Bibi, E. (2018) A new critical conformational determinant of multidrug efflux by an MFS transporter. *J. Mol. Biol.* **430,** 1368–1385 CrossRef Medline
42. Drew, D., and Boudker, O. (2016) Shared molecular mechanisms of membrane transporters. *Annu. Rev. Biochem.* **85,** 543–572 CrossRef Medline
43. Brill, S., Falk, O. S., and Schuldiner, S. (2012) Transforming a drug/H^+ antiporter into a polyamine importer by a single mutation. *Proc. Natl. Acad. Sci. U.S.A.* **109,** 16894–16899 CrossRef Medline
44. Morrison, E. A., and Henzler-Wildman, K. A. (2012) Reconstitution of integral membrane proteins into isotropic bicelles with improved sample stability and expanded lipid composition profile. *Biochim. Biophys. Acta* **1818,** 814–820 CrossRef Medline

The C terminus of the bacterial multidrug transporter EmrE couples drug binding to proton release

Nathan E. Thomas, Chao Wu, Emma A. Morrison, Anne E. Robinson, Josephine P. Werner and Katherine A. Henzler-Wildman

J. Biol. Chem. 2018, 293:19137-19147.
doi: 10.1074/jbc.RA118.005430 originally published online October 4, 2018